Drain Current Model Including Velocity Saturation for Symmetric Double-Gate MOSFETs

Venkatnarayan Hariharan, *Student Member, IEEE*, Juzer Vasi, *Fellow, IEEE*, and V. Ramgopal Rao, *Senior Member, IEEE*

***Abstract*—A drain current model is developed for a symmetrically driven undoped (or lightly doped) symmetric double-gate MOSFET (SDGFET) under the drift–diffusion transport mechanism, with velocity saturation effects being included as an integral part of the model derivation. Velocity saturation effects are modeled by using the Caughey–Thomas engineering model with exponent $n = 2$. I_d–V_d, I_d–V_g, g_m–V_g, and $g_{\rm DS}$–V_d comparisons are made with 2-D device simulation results, and a very good match is found all the way from subthreshold to strong inversion. Gummel symmetry compliance is also shown.**

***Index Terms*—Current, double-gate MOSFET (DGFET), mobility, modeling, MOSFETs, velocity saturation.**

NOMENCLATURE

$\Psi(x, y)$	Electrostatic potential (with respect to $\varphi_{\rm fn}$ in the source end).
$\varphi_{\rm fn}(x)$	Electron quasi-Fermi potential ($= 0$ at the source end).
q	Electronic charge.
Φ_t	Thermal voltage (kT/q).
$\Delta\varphi$	Model parameter: work function difference between the gate electrodes and intrinsic silicon.
$v_{\rm sat}$	Model parameter: saturation velocity.
$V_{\rm DSat}$, $I_{\rm DSat}$	Drain saturation voltage, current.
Q_i	Inversion-charge areal density.
$\beta_1(\beta_{1s}, \beta_{1d})$	Intermediate constant (β_{1s} and β_{1d} are its values at the source and drain ends, respectively).
$\beta_2(\beta_{2s}, \beta_{2d})$	Intermediate constant (β_{2s} and β_{2d} are its values at the source and drain ends, respectively).
$E_{\rm xs}$	Lateral electric field at the oxide–silicon interface.
$C_{\rm ox}$	Gate oxide capacitance per unit area.
$t_{\rm ox}$	Gate oxide thickness.
ε, $\varepsilon_{\rm ox}$	Silicon permittivity, gate oxide permittivity.
μ_0	Model parameter: base mobility in the absence of any velocity saturation.
$W_{\rm fin}$	Fin width (i.e., distance between the closest edges of the front and back gate oxides).
L	Metallurgical channel length.
$I_{\rm DS}$	Drain current.
$I_{\rm DS0}$	Drain current in the absence of any velocity saturation effects.
$E_{\rm sat}$	Model parameter: lateral electric field at the onset of velocity saturation.
ΔL	Extent of channel length modulation (CLM).

Manuscript received March 25, 2008. This paper was supported in part by an Intel academic grant. The review of this paper was arranged by Editor C. McAndrew.

The authors are with the Department of Electrical Engineering, Indian Institute of Technology Bombay, Mumbai 400 076, India (e-mail: vharihar@ee.iitb.ac.in; vasi@ee.iitb.ac.in; rrao@ee.iitb.ac.in).

Color versions of one or more of the figures in this paper are available online at http://ieeexplore.ieee.org.

Digital Object Identifier 10.1109/TED.2008.926745

I. INTRODUCTION

IN THE PAST few decades, semiconductor technology has successfully continued forth with the conventional scaling approach to shrink devices. However, technology scaling of the conventional MOSFET is reaching a point where there are numerous issues with it going forward, and any suggested work-around has some other problem linked to it. As a result, alternate structures have been studied for quite a while now. One such structure is the double-gate MOSFET (DGFET), a practical realization of which is via the double-gate FinFET. DGFETs are more amenable to scaling compared with the conventional MOSFETs by virtue of their better electrostatics [1], [2]. Also, as devices shrink, adjusting their threshold voltage by doping the channel is not an acceptable option because doping presents problems like random dopant fluctuations and also degrades the channel mobility. Hence, it is of special interest to model undoped DGFETs. A DGFET with identical material and thickness for the front and back gate electrodes and dielectric is called a symmetric DGFET (SDGFET).

There have been many efforts to model the drain current for DGFETs. In [3], [4] charge sheet models were used, whereas in [4]–[12], and [28], a constant mobility was assumed. References [3] and [13] considered velocity saturation effects by using the Caughey–Thomas model [17] or its variants with exponent $n = 1$ (the variants (e.g., [14]) differing in the way the critical electric field E_c relates to $v_{\rm sat}$, but all of them, nevertheless, using an exponent $n = 1$). In [15], which used the velocity saturation model as described in [16], the Caughey–Thomas model with exponent $n = 2$ was used; however, the spatial variation of the driving electric field was not retained in the core model formulation. To the authors' best knowledge, there has been no work done on modeling velocity saturation effects in DGFETs by using the Caughey–Thomas model with exponent $n = 2$, where velocity saturation effects are included as an integral part of the model derivation. The key novelty in this paper is that the spatial variation of the lateral electric field driving the velocity saturation effect is represented accurately in the core model derivation. Hence, our model is expected to be physically more accurate, particularly for shorter channel

devices where velocity saturation effects are significant, and this is discussed in Section VI.

Using an exponent $n = 2$ has been found to yield a better match with experimental data for n-channel devices [18]. Furthermore, it has been suggested [19] that using an exponent $n = 1$, or any odd number, would yield a model that would fail the Gummel symmetry test at $V_{\rm DS} = 0$. Because of this, some models use $n = 2$ for conventional MOSFETs for n-and p-channel devices [20], [16] (Gildenblat *et al.* [16] actually use an adjusted form of the Scharfetter–Gummel model for velocity saturation which simplifies to the Caughey–Thomas model with $n = 2$, except that the saturation velocity parameter $v_{\rm sat}$ becomes bias dependent in the case of p-channel devices). Even though efforts after [17] such as the Canali model [21] have found a good experimental fit using fractional values for exponent n between one and two, their work showed that the exponent n increases (toward two) at temperatures higher than room temperature. Then, considering the fact that fractional exponents are hard to accommodate in a compact model derivation and that the operating temperatures, specifically of high-speed devices, are higher than room temperature, and that the Caughey–Thomas exponent is usually not a temperature-scaled parameter in compact models, this lends further justification for modeling velocity saturation using an exponent $n = 2$ in a compact model.

Threshold-voltage-based models are not very physical [16], and charge sheet models are not very valid in ultrathin DGFETs as they fail to model phenomena such as volume inversion [5]. Hence, in this paper, we develop an inversion-charge-based drain current model. We do this by solving for the drain current $(I_{\rm DS})$ of an undoped/lightly doped SDGFET under the gradual channel approximation (GCA), considering the intrinsic portion of the device. We have focused on mobility degradation due to velocity saturation, and other mobility degradation effects, such as that due to the vertical field, have not been considered in this paper.

Finally, we present I_d–V_d, I_d–V_g, g_m–V_g, and $g_{\rm DS}$–V_d comparisons between our model and 2-D device simulation results. We also show Gummel symmetry compliance [19] of our model.

II. Basic Formulation

The schematic of the intrinsic portion of an n-channel SDGFET is shown in Fig. 1. Under the GCA and neglecting the body doping term, the 1-D Poisson equation can be written as

$$\frac{\partial^2 \psi}{\partial y^2} = \frac{qn_i}{\varepsilon} e^{(\psi - \phi_{\rm fn})/\phi_t}. \tag{1}$$

Proceeding as in [5], this can be solved to yield

$$\begin{aligned} f(\beta_1) &= 0 \\ &= \frac{4\varepsilon\phi_t\beta_1 \tan(\beta_1)}{W_{\rm fin}C_{\rm ox}} + \phi_{\rm fn} \\ &\quad + 2\phi_t \ln\left(\frac{2\beta_1 \sec(\beta_1)}{\beta W_{\rm fin}}\right) - (V_{\rm GS} - \Delta\phi) \end{aligned} \tag{2}$$

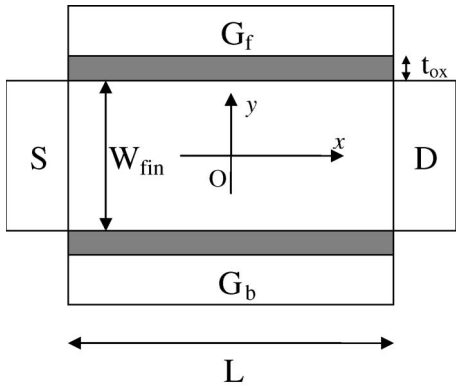

Fig. 1. Schematic of an SDGFET, showing the coordinate axes and the dimensions labeled. The source- and drain-body junctions are assumed to be abrupt.

where β_1 is a state variable and is the same as β in [5]. It is related to the inversion-charge areal density

$$Q_i = \frac{-8\varepsilon\phi_t\beta_1 \tan(\beta_1)}{W_{\rm fin}} \tag{3}$$

and β is given by

$$\beta = \sqrt{\frac{qn_i}{2\varepsilon\phi_t}}. \tag{4}$$

Note that (2) is the same as [5, eq. (4)]. Using (2), we can, in principle, determine β_1 at the source and drain ends by setting $\varphi_{\rm fn} = 0$ and $\varphi_{\rm fn} = V_{\rm DS}$, respectively. We will refer to these as β_{1s} and β_{1d}, respectively. An approximated form of (2) is [13]

$$\begin{aligned} f(\beta_1) &= 0 \\ &= \frac{4\varepsilon\phi_t\beta_1 \tan(\beta_1)}{W_{\rm fin}C_{\rm ox}} + \phi_{\rm fn} \\ &\quad + \phi_t \ln\left(\frac{4\left(\beta_1 \tan(\beta_1) + \beta_1^2 \tan^2(\beta_1)\right)}{\beta^2 W_{\rm fin}^2}\right) \\ &\quad - (V_{\rm GS} - \Delta\phi). \end{aligned} \tag{5}$$

Recently, there have also been closed-form approximate solutions to (2) [29].

Now, in the drift–diffusion model, the drain current per unit fin height is

$$I_{\rm DS} = -\mu_{\rm eff}(x) Q_i(x) \frac{d\phi_{\rm fn}}{dx}. \tag{6}$$

We model velocity saturation effects by using the Caughey–Thomas model [17] with exponent $n = 2$ as

$$\mu_{\rm eff}(x) = \frac{\mu_0}{\sqrt{1 + \frac{\mu_0^2 E_{\rm xs}^2}{v_{\rm sat}^2}}}. \tag{7}$$

In (7), we choose to model the driving field E_x as being the lateral field at the oxide–silicon interface E_{xs}. This is not unreasonable because, even though charge sheet models

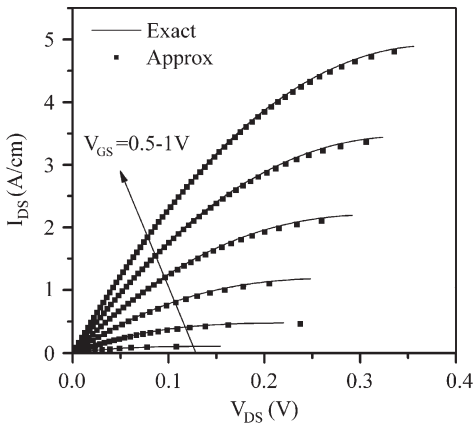

Fig. 2. I_d–V_d plot by numerically solving (2) and (9) using a constant $I_{\rm DS}$ step size (with and without the approximation stated in the first paragraph of Section III).

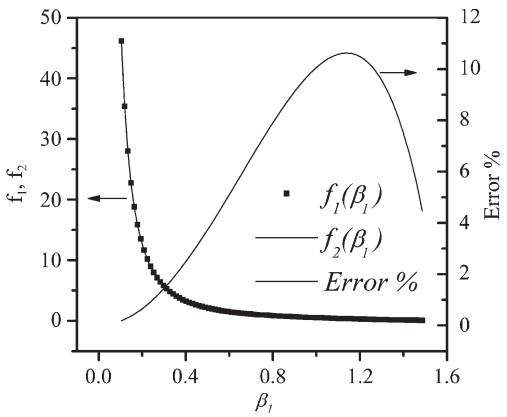

Fig. 3. Comparison of $f_1(\beta_1)$ and $f_2(\beta_1)$.

are invalid in DGFETs [5] and there is nonnegligible current flowing even far from the oxide–silicon interface, the current at the interface is still dominant (except in the subthreshold regime [22] where the leakiest path is along the fin center. However, as we will see, our model predicts the current quite well in the subthreshold regime also). From the 1-D Poisson solution, one can easily show that

$$E_{\rm xs}(\beta_1(x)) = -\frac{\partial\psi(x, W_{\rm fin}/2)}{\partial x} = \frac{4\varepsilon\phi_t}{W_{\rm fin}C_{\rm ox}}\left(\beta_1(x)\sec^2\beta_1(x)+\tan\beta_1(x)\right)\frac{d\beta_1(x)}{dx}. \tag{8}$$

Using (8) in (7) and proceeding on the same lines as in [5], we finally get (9), shown at the bottom of the page.

The limiting case of (9) for the constant mobility case (for $v_{\rm sat} = \infty$) can be recognized as the exact same equation derived in [5], which had considered mobility to be constant. Equations (2) and (9) are the key equations in our approach. An I_d–V_d plot generated by numerically solving (2) and (9) in Scilab [23] by ramping $I_{\rm DS}$ is shown in Fig. 2.

Equation (9) is not easily integrable, so we make some approximations in order to proceed.

III. Approximations

In (9), let us denote the $(1+\beta_1\tan\beta_1)/\beta_1$ term by t_{12}. If this term t_{12} is multiplied by $1-((\tan\beta_1-\beta_1)/(2+\beta_1\tan\beta_1)\tan\beta_1)$, then the analytics becomes simpler. Before proceeding with the simplified analytics, the origin and justification of this approximation is explained first.

A. Origin and Justification of the Approximation

In (9), there is a maximum value of $I_{\rm DS}$ beyond which the integrand becomes imaginary. This extreme point is the limit of validity of the model. The limiting $V_{\rm DS}$ that causes this extremum is $V_{\rm DSat}$.

By setting the integrand in (9) to zero, the limiting $I_{\rm DS}(I_{\rm DS\,max})$ is obtained as

$$I_{\rm DS\,max} = 4\phi_t\beta_1\tan\beta_1 C_{\rm ox}v_{\rm sat} \times\left[\frac{2\varepsilon}{W_{\rm fin}C_{\rm ox}}+\frac{1+\beta_1\tan\beta_1}{\beta_1(\beta_1\sec^2\beta_1+\tan\beta_1)}\right]. \tag{10}$$

The second term in (10) can be rewritten as

$$f_1(\beta_1) = \frac{1+\beta_1\tan\beta_1}{\beta_1^2+(1+\beta_1\tan\beta_1)\beta_1\tan\beta_1}. \tag{11}$$

Compare this to

$$f_2(\beta_1) = \frac{1+\beta_1\tan\beta_1}{\beta_1\tan\beta_1+(1+\beta_1\tan\beta_1)\beta_1\tan\beta_1}. \tag{12}$$

$f_1(\beta)$ and $f_2(\beta)$ are shown in Fig. 3. We see a reasonably good match, with a maximum error of about 10% and an average error of about 6%. This approximation is equivalent to making the approximation that is stated in the first paragraph of Section III. As a further validation of this approximation, the I_d–V_d plots have been regenerated using Scilab by numerically solving (2) and (9) but, this time, using this approximation, and they are shown in Fig. 2. We can clearly see a very close match.

$$-\frac{W_{\rm fin}}{4\mu_0\varepsilon\phi_t}\left(x+\frac{L}{2}\right) = \int_{\beta_{1s}}^{\beta_1}\left\{\frac{16\phi_t^2\beta_1^2\tan^2\beta_1}{I_{\rm DS}^2}\left[\frac{2\varepsilon}{W_{\rm fin}C_{\rm ox}}(\beta_1\sec^2\beta_1+\tan\beta_1)+\frac{1+\beta_1\tan\beta_1}{\beta_1}\right]^2-\frac{(\beta_1\sec^2\beta_1+\tan\beta_1)^2}{C_{\rm ox}^2v_{\rm sat}^2}\right\}^{1/2}d\beta_1 \tag{9}$$

B. Use of the Approximation

By using this approximation, (9) can be simplified as

$$\frac{-W_{\rm fin}}{4\mu_0\varepsilon\phi_t}\left(x+\frac{L}{2}\right) \cong \int_{\beta_{2s}}^{\beta_2}\sqrt{\frac{16\phi_t^2\beta_2^2}{I_{\rm DS}^2}\left[\frac{2\varepsilon}{W_{\rm fin}C_{ox}}+\frac{1+\beta_2}{(2+\beta_2)\beta_2}\right]^2-\frac{1}{C_{\rm ox}^2v_{\rm sat}^2}}d\beta_2 \tag{13}$$

where we have changed from the state variable β_1 to β_2 that is given by

$$\beta_2=\beta_1\tan\beta_1. \tag{14}$$

Equation (13) is still not easily integrable, and we need to make further approximations. Making the approximation that the second term in the integrand $1/C_{\rm ox}^2v_{\rm sat}^2$ is small, this can be integrated to get

$$I_{\rm DS}=\frac{8a_1(x)\phi_t}{\frac{W_{\rm fin}(x+L/2)}{4\mu_0\varepsilon\phi_t}+\sqrt{\left(\frac{W_{\rm fin}(x+L/2)}{4\mu_0\varepsilon\phi_t}\right)^2+\frac{a_1(x)a_2(x)}{b\cdot C_{\rm ox}^2v_{\rm sat}^2}}} \tag{15}$$

where

$$a_1(x)=\frac{b}{2}\left(\beta_{2s}^2-\beta_2(x)^2\right)+(\beta_{2s}-\beta_2(x))-\ln\left(\frac{\beta_{2s}+2}{\beta_2(x)+2}\right)$$

$$a_2(x)=\frac{(2b-1)}{\sqrt{4b^2+1}} \times\ln\left\{\frac{\left[\frac{2b(\beta_{2s}+1)+1}{\sqrt{4b^2+1}}+1\right]\cdot\left[\frac{2b(\beta_2(x)+1)+1}{\sqrt{4b^2+1}}-1\right]}{\left[\frac{2b(\beta_{2s}+1)+1}{\sqrt{4b^2+1}}-1\right]\cdot\left[\frac{2b(\beta_2(x)+1)+1}{\sqrt{4b^2+1}}+1\right]}\right\} +\ln\left(\frac{b\beta_{2s}^2+(2b+1)\beta_{2s}+1}{b\beta_2(x)^2+(2b+1)\beta_2(x)+1}\right) \tag{16}$$

$$b=\frac{2\varepsilon}{W_{\rm fin}C_{\rm ox}}. \tag{17}$$

The drain current $I_{\rm DS}$ expression can then be derived by setting $x=L/2$ in (15) and $\beta_2=\beta_{2d}$ in the expressions for a_1 and a_2 in (16) (and calling them a_{1d} and a_{2d}, respectively). We get

$$I_{\rm DS}=\frac{2I_{\rm DS0}}{1+\sqrt{1+\frac{8\mu_0^2\varepsilon\phi_t^2a_{1d}a_{2d}}{W_{\rm fin}L^2C_{\rm ox}v_{\rm sat}^2}}} \tag{18}$$

$$I_{\rm DS0}=\frac{16\mu_0\varepsilon\phi_t^2a_{1d}}{W_{\rm fin}L} \tag{19}$$

where $I_{\rm DS0}$ is the current in the absence of velocity saturation (constant mobility current). $I_{\rm DS}$ in (18) can be further simplified by considering that the second term in the square root is small (meaning large $v_{\rm sat}$). We then get

$$I_{\rm DS}=\frac{I_{\rm DS0}}{1+\frac{I_{\rm DS0}\mu_0a_{2d}}{8C_{\rm ox}v_{\rm sat}^2L}}. \tag{20}$$

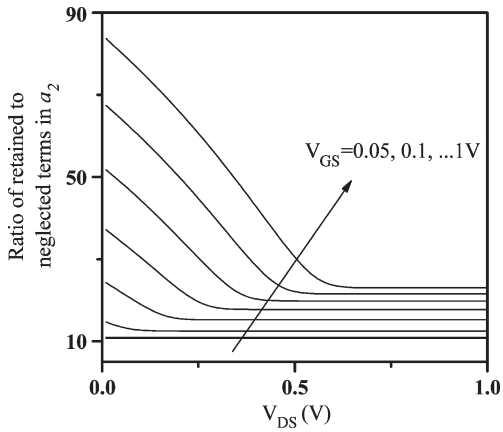

Fig. 4. Ratio of the retained terms to the neglected terms in a_2 for the $L=30$-nm device. $V_{\rm GS}=0.05, 0.1, 0.2, \ldots, 1$ V.

Furthermore, the first logarithm term in a_2 in (16) is negligible. Thus, a_{1d} and a_{2d} can be written as

$$a_{1d}=\frac{b}{2}\left(\beta_{2s}^2-\beta_{2d}^2\right)+(\beta_{2s}-\beta_{2d})-\ln\left(\frac{\beta_{2s}+2}{\beta_{2d}+2}\right)$$

$$a_{2d}=\ln\left(\frac{b\beta_{2s}^2+\beta_{2s}(2b+1)+1}{b\beta_{2d}^2+\beta_{2d}(2b+1)+1}\right). \tag{21}$$

The ratio of the dominant (retained) terms and the neglected terms [in arriving from (16) to (21)] is shown in Fig. 4 for a $L=30$-nm, $W_{\rm fin}=10$-nm, and $t_{\rm ox}=1$-nm device. As can be clearly seen, the approximation is quite valid.

Equations (19)–(21) are the final drain current equations in our model.

IV. Drain Saturation Voltage $V_{\rm DSat}$

To find $V_{\rm DSat}$, we first model the drift component. For this, we follow the same approach as described in the previous sections, except that we only consider the drift component $I_{\rm DS}^{\rm drift}$ (as also done in MOS Model 11 [24]), and we make the approximation [in the equation that is equivalent to (9)] that $I_{\rm DS}^{\rm drift}$ is spatially constant, which is a valid approximation in strong inversion because majority of the current is then due to drift. We then set $\partial I_{\rm DS}^{\rm drift}/\partial V_{\rm DS}=0$. By doing so, we get

$$\beta_{\rm 2dsat}=\frac{\sqrt{1+2bk\beta_{2s}^2}-1}{\sqrt{2bk}} \tag{22}$$

where

$$k=\frac{2\mu_0^2\varepsilon\phi_t^2}{W_{\rm fin}L^2C_{\rm ox}v_{\rm sat}^2}. \tag{23}$$

For a given $V_{\rm GS}$, the quantities β_{1s} and β_{2s} can be calculated in order by using (2) and (14), respectively, and (22) can then be solved in closed form for $\beta_{\rm 2dsat}$, from which $V_{\rm DSat}$ can be calculated in closed form by using (5) and (14).

Having found V_{DSat}, a V_{DSeff} can be defined [20] in order to smoothly vary between the transition regions and limit V_{DS} at V_{DSat} when it exceeds V_{DSat}

$$V_{\mathrm{DSeff}} = V_{\mathrm{DS}} \left(1 + \left(\frac{V_{\mathrm{DS}}}{V_{\mathrm{DSat}}} \right)^{\mathrm{AX}} \right)^{-1/\mathrm{AX}} \tag{24}$$

where AX is a model parameter.

V. Channel Length Modulation (CLM)

To model CLM in the post-velocity saturation regime, we have used an approach that is similar to that of Ko *et al.* [25] and Taur and Ning [18] and applied it to a DGFET. The CLM expression is

$$\Delta L = l \cdot \ln \left[\frac{V_{\mathrm{DS}} - V_{\mathrm{DSat}}}{l \cdot E_{\mathrm{sat}}} + \sqrt{\left(\frac{V_{\mathrm{DS}} - V_{\mathrm{DSat}}}{l \cdot E_{\mathrm{sat}}} \right)^2 + 1} \right] \tag{25}$$

where

$$l = \sqrt{\frac{\varepsilon W_{\mathrm{fin}}}{2C_{\mathrm{ox}}}}. \tag{26}$$

In our model implementation, in (25), we replaced the V_{DSat} term with V_{DSeff} as defined in (24) in order to have a nonzero ΔL only when $V_{\mathrm{DS}} > V_{\mathrm{DSat}}$. Also, we replaced L in (19) by $L_{\mathrm{eff}} = L - \Delta L$.

VI. Comparison With Device Simulations

Two-dimensional device simulations were done on an n-channel SDGFET by using Synopsis Sentaurus Device [26]. The device structure was created with abrupt source- and drain-body junctions. The body was lightly doped at 10^{15} cm^{-3} p-type, and the source and drain regions were kept short in length and were doped at 10^{19} cm^{-3} n-type. In order to focus on just the mobility degradation due to the lateral field, other models were disabled, such as vertical-field mobility degradation, doping-dependant mobility, etc. Recombination–generation models, quantum–mechanical models, etc., were also turned off. A midgap work function with a zero barrier with respect to intrinsic silicon was used for the gate electrode, and the basal mobility was downgraded to 300 cm^2/V $\cdot$ s in order to emulate realistic vertical-field-degraded mobilities. Default values were used for all the other parameters. Thus, the saturation velocity and the Caughey–Thomas exponent used by the device simulator were 1.07×10^7 cm/s and 1.11, respectively.

Device simulations were done for two channel lengths, namely, 1) $L_g = 100$ nm, $W_{\mathrm{fin}} = 10$ nm, and $T_{\mathrm{ox}} = 1$ nm and 2) $L_g = 200$ nm, $W_{\mathrm{fin}} = 10$ nm, and $T_{\mathrm{ox}} = 1$ nm, and the results were compared with the analytical model. The gate oxide thicknesses have been chosen to reduce 2-D field effects, such as DIBL, since these effects have not been incorporated in the core model formulation.

A comparison of various models, including our model, is shown in Fig. 5. In doing this comparison, the various analytical models used the same parameter values as those used in the device simulations. In all the models shown in that figure, the drain current was clamped at the point of zero slope (I_{DSat}),

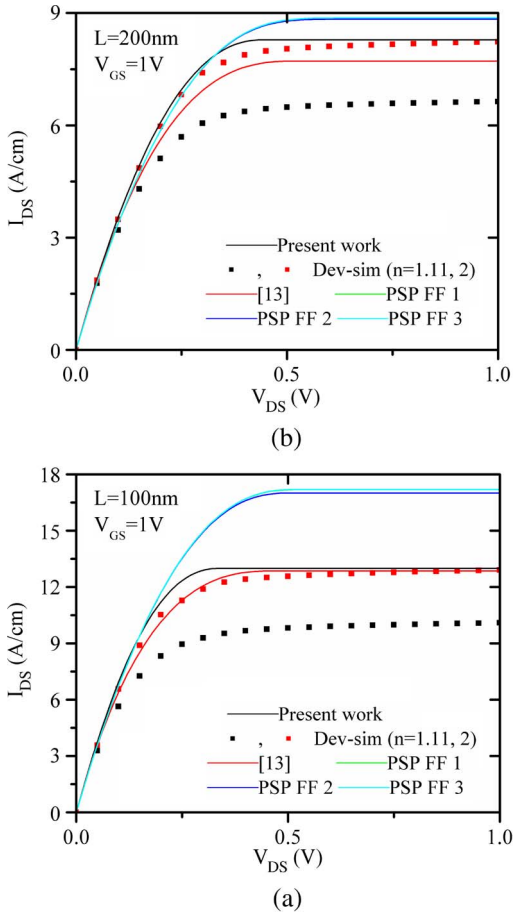

Fig. 5. Comparison of various models at $V_{\mathrm{GS}} = 1$ V. The symbols are for the device simulation curves with two different values for the Caughey–Thomas exponent, namely, $n = 1.11$ (the default) and $n = 2$. The device simulation curves and the analytical model curves use the same parameter values.

simply by detecting the onset of droop in I_{DS}. It was not done by using (24) in order to avoid ambiguities related to extracted parameters (such as the proper value of AX to use), when drawing conclusions from the comparison. The clamping was done in order to avoid the unphysical negative output conductance that is otherwise visible in all the models (which is a known result [20], [30] when modeling velocity saturation), and one should interpret the models only until the point of zero slope and not beyond that. In Fig. 5, the curves labeled [13] are based on [13, eq. (20)]. The curves labeled *PSP FF 1–3* use the drain current equation from the PSP-FinFET model [15, eqs. (28)–(30)] with low-field mobility turned off ($G_{\mathrm{mob}} = 1$) and using the theoretical value of $\theta_{\mathrm{sat}} = \mu_0/(Lv_{\mathrm{sat}})$. Specifically, the curves labeled *PSP FF 1* use a uniform driving field for velocity saturation [24, eq. (3.44)]. The curves labeled *PSP FF 2* use a linearly varying driving field for velocity saturation [24, eqs. (3.45 and 3.46)]. The curves labeled *PSP FF 3* use an expression for G_{vsat} as defined in PSP 102.2 ([27, eqs. (4.144) and (4.145)] with $\boldsymbol{THESATG} = 0$ and $G_{\Delta L} = 1$). As can be seen from Fig. 5, compared to the PSP-FinFET model (which is, to the best of our knowledge, the only other DGFET model besides our model which assumes $n = 2$ in the velocity saturation model), our model curves are closer to the $n = 1.11$ device simulation curves. Furthermore, this

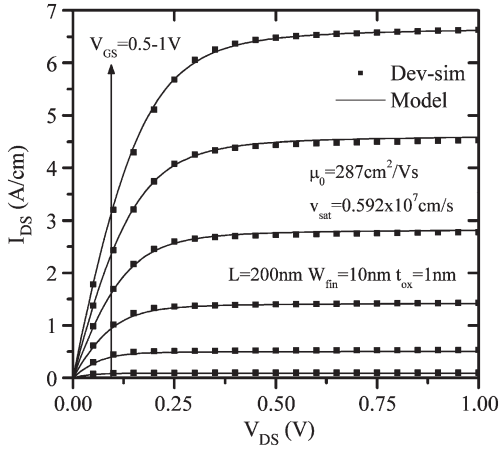

Fig. 6. Output characteristics for the $L = 200$-nm device. Values of key parameters used by the model are shown in the figure.

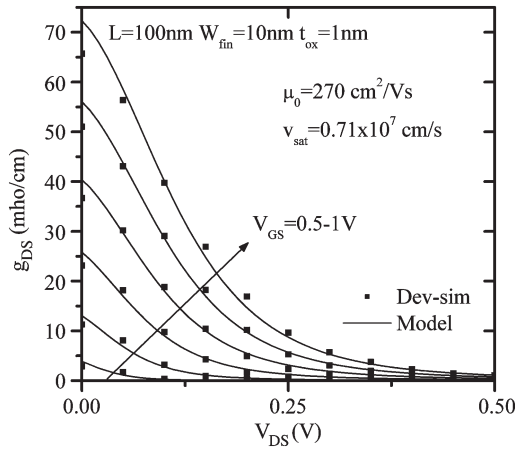

Fig. 7. Output conductance for the $L = 100$-nm device. Values of key parameters used by the model are shown in the figure.

difference is more pronounced for the shorter channel length device where velocity saturation effects are more significant. Also, compared to the PSP-FinFET model curves, our model curves are closer to the $n = 2$ device simulation curve, thereby being in agreement with the underlying premise of $n = 2$ in the model formulation. It can also be seen that the curves for the model developed in [13] are closer to the $n = 1.11$ device simulation curves when compared to our model. This is an expected result because a value of $n = 1$ was assumed in [13], which is closer (than the value of $n = 2$ as used by us) to the default $n = 1.11$ used in the device simulator. However, as stated before, a model developed by using $n = 1$ would not be Gummel symmetric at $V_{\rm DS} = 0$, and this has been verified by us for the model developed in [13].

A sampling of I_d–V_d, $g_{\rm DS}$–V_d, I_d–V_g, and g_m–V_g characteristics for each device is shown in Figs. 6–9. All quantities are per unit fin height. The parameters μ_0, $v_{\rm sat}$, $E_{\rm sat}$, and AX were extracted from the corresponding device simulation data by using a parameter extraction program developed at the Indian Institute of Technology Bombay, Mumbai, India [31]. The extracted values were $\mu_0 = 270$ cm^2/V $\cdot$ s, $v_{\rm sat} = 0.71 \times 10^7$ cm/s, $E_{\rm sat} = 4.3 \times 10^6$ V/cm, and AX $= 2$ for the 100-nm device and $\mu_0 = 287$ cm^2/V $\cdot$ s, $v_{\rm sat} = 0.592 \times 10^7$ cm/s,

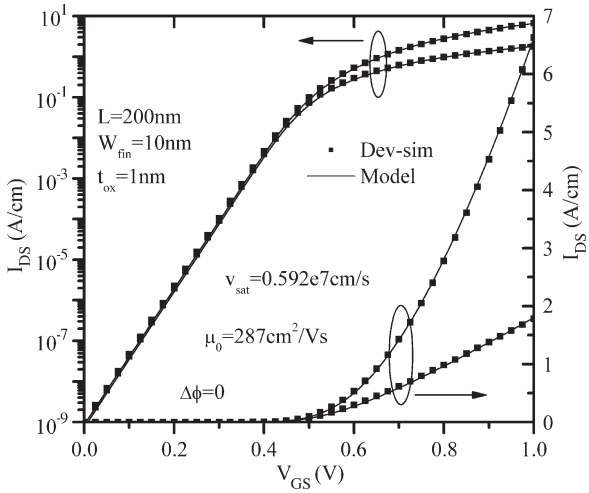

Fig. 8. Transfer characteristics for the $L = 200$-nm device at $V_{\rm DS} = 50$ mV and $V_{\rm DS} = 1$ V. Values of key parameters used by the model are shown in the figure.

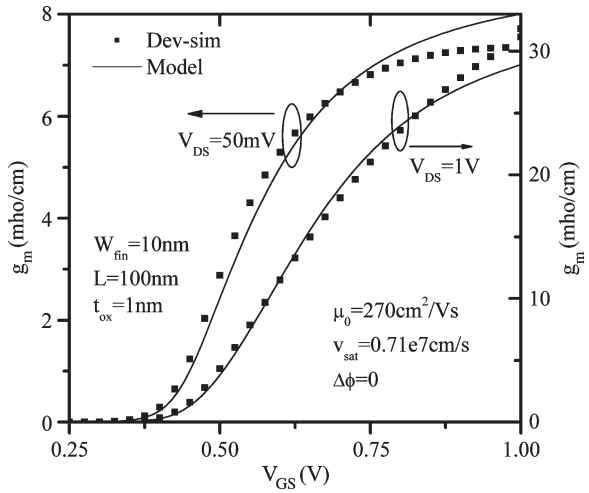

Fig. 9. Transconductance of the $L = 100$-nm device at $V_{\rm DS} = 50$ mV and $V_{\rm DS} = 1$ V. Values of key parameters used by the model are shown in the figure.

$E_{\rm sat} = 9.7 \times 10^6$ V/cm, and AX $= 2.51$ for the 200-nm device. The extracted values for μ_0, $v_{\rm sat}$, and AX are used in the respective analytical model curves shown in Figs. 6–9. For the remaining parameters, the analytical model uses a fixed $\Delta\varphi = 0$ V (same as that used in the device simulations) and a fixed value for the CLM parameter $E_{\rm sat} = 4.3 \times 10^6$ V/cm (namely, the one extracted for the 100-nm device) for both channel length devices. The extracted basal mobilities are thus not far from the value of 300 cm^2/V $\cdot$ s used in the device simulator. Moreover, as can be seen from Figs. 6–9, the analytical versus device simulation matching is very good.

Last, Gummel symmetry compliance of our model was tested by following the procedure described in [19]. As expected, our model is symmetric, and the results are shown in Fig. 10.

VII. Conclusion

A single-equation (i.e., not piecewise) drain current model considering velocity saturation has been developed for an

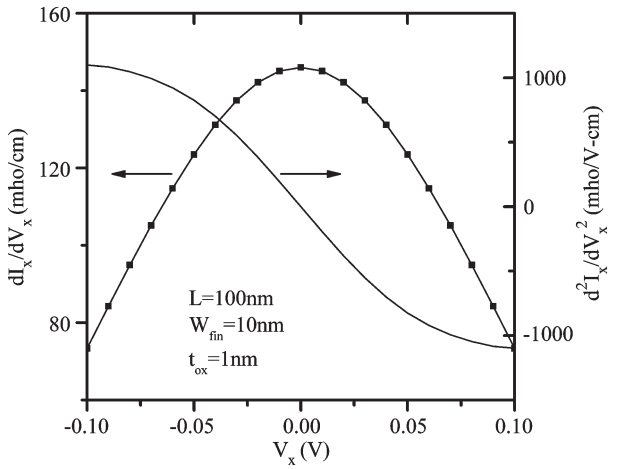

Fig. 10. Gummel symmetry tests [19] show model symmetry with respect to $V_{\rm DS} = 0$. The symbols are a flipped version of the line.

undoped or lightly doped SDGFET based on the drift–diffusion transport mechanism, using an exponent $n = 2$ for velocity saturation as an integral part of the model derivation. The model is inversion charge based, is valid in subthreshold as well as in above threshold, and is symmetric about the $V_{\rm DS} = 0$ point. Analytical versus 2-D device simulation comparisons were done, and a very good match was found.

From a compact-model implementation standpoint, terminal charge calculations also need to be formulated for quasi-static ac analysis. Also, additional physical effects, such as 2-D field effects (DIBL), quantum effects, vertical-field mobility degradation effects, etc., need to be incorporated into it in order to build a complete compact model.

ACKNOWLEDGMENT

The authors would like to thank Synopsys, Inc. for the TCAD tool support.

REFERENCES

[1] P. M. Solomon, K. W. Guarini, Y. Zhang, K. Chan, E. C. Jones, G. M. Cohen, A. Krasnoperova, M. Ronay, O. Dokumaci, and H. J. Hovel, "Two gates are better than one," *IEEE Circuits Devices Mag.*, vol. 19, no. 1, pp. 48–62, Jan. 2003.

[2] E. J. Nowak, I. Aller, T. Ludwig, K. Kim, R. V. Joshi, C.-T. Chuang, K. Bernstein, and R. Puri, "Turning silicon on its edge," *IEEE Circuits Devices Mag.*, vol. 20, no. 1, pp. 20–31, Jan./Feb. 2004.

[3] G. Pei, W. Ni, A. V. Kammula, B. A. Minch, and E. C.-C. Kan, "A physical compact model of DG MOSFET for mixed-signal circuit applications—Part I: Model description," *IEEE Trans. Electron Devices*, vol. 50, no. 10, pp. 2135–2143, Oct. 2003.

[4] M. V. Dunga, C. H. Lin, X. Xi, D. D. Lu, A. M. Niknejad, and C. Hu, "Modeling advanced FET technology in a compact model," *IEEE Trans. Electron Devices*, vol. 53, no. 9, pp. 1971–1978, Sep. 2006.

[5] Y. Taur, X. Liang, W. Wang, and H. Lu, "A continuous, analytic drain-current model for DG MOSFETs," *IEEE Electron Device Lett.*, vol. 25, no. 2, pp. 107–109, Feb. 2004.

[6] J. He, X. Xuemei, M. Chan, C. H. Lin, A. M. Niknejad, and C. Hu, "A non-charge-sheet based analytical model of undoped symmetric double-gate MOSFETs using SPP approach," in *Proc. Int. Symp. Quality Electron. Des.*, 2004, pp. 45–50.

[7] J. M. Sallese, F. Krummenacher, F. Pregaldiny, C. Lallement, A. Roy, and C. C. Enz, "A design oriented charge-based current model for symmetric DG MOSFET and its correlation with the EKV formalism," *Solid State Electron.*, vol. 49, no. 3, pp. 485–489, Mar. 2005.

[8] A. S. Roy, J. M. Sallese, and C. C. Enz, "A closed-form charge-based expression for drain current in symmetric and asymmetric double gate MOSFET," *Solid State Electron.*, vol. 50, no. 4, pp. 687–693, Apr. 2006.

[9] H. Lu and Y. Taur, "An analytic potential model for symmetric and asymmetric DG MOSFETs," *IEEE Trans. Electron Devices*, vol. 53, no. 5, pp. 1161–1168, May 2006.

[10] A. Ortiz-Conde, F. J. G. Sanchez, and J. Muci, "Rigorous analytic solution for the drain current of undoped symmetric dual-gate MOSFETs," *Solid State Electron.*, vol. 49, no. 4, pp. 640–647, Apr. 2005.

[11] J. He, F. Liu, J. Zhang, J. Feng, J. Hu, S. Yang, and M. Chan, "A carrier-based approach for compact modeling of the long-channel undoped symmetric double-gate MOSFETs," *IEEE Trans. Electron Devices*, vol. 54, no. 5, pp. 1203–1209, May 2007.

[12] Z. Zhu, X. Zhou, S. C. Rustagi, G. H. See, S. Lin, G. Zhu, C. Wei, and J. Zhang, "Analytic and explicit current model of undoped double-gate MOSFETs," *Electron. Lett.*, vol. 43, no. 25, pp. 1464–1466, Dec. 2007.

[13] M. Wong and X. Shi, "Analytical I–V relationship incorporating field-dependent mobility for a symmetrical DG MOSFET with an undoped body," *IEEE Trans. Electron Devices*, vol. 53, no. 6, pp. 1389–1397, Jun. 2006.

[14] C. G. Sodini, P.-K. Ko, and J. L. Moll, "The effect of high fields on MOS device and circuit performance," *IEEE Trans. Electron Devices*, vol. ED-31, no. 10, pp. 1386–1393, Oct. 1984.

[15] G. D. J. Smit, A. J. Scholten, G. Curatola, R. van Langevelde, G. Gildenblat, and D. B. M. Klaassen, "PSP-based scalable compact FinFET model," in *Proc. NSTI-Nanotech*, 2007, vol. 3, pp. 520–525.

[16] G. Gildenblat, X. Li, W. Wu, H. Wang, A. Jha, R. van Langevelde, G. D. J. Smit, A. J. Scholten, and D. B. M. Klaassen, "PSP: An advanced surface-potential-based MOSFET model for circuit simulation," *IEEE Trans. Electron Devices*, vol. 53, no. 9, pp. 1979–1993, Sep. 2006.

[17] D. M. Caughey and R. E. Thomas, "Carrier mobilities in silicon empirically related to doping and field," *Proc. IEEE*, vol. 55, no. 12, pp. 2192–2193, Dec. 1967.

[18] Y. Taur and T. Ning, *Fundamentals of Modern VLSI Devices*. Cambridge, U.K.: Cambridge Univ. Press, 2003.

[19] K. Joardar, K. K. Gullapalli, C. C. McAndrew, M. E. Burnham, and A. Wild, "An improved MOSFET model for circuit simulation," *IEEE Trans. Electron Devices*, vol. 45, no. 1, pp. 134–148, Jan. 1998.

[20] G. Gildenblat, H. Wang, T.-L. Chen, X. Gu, and X. Cai, "SP: An advanced surface-potential-based compact MOSFET model," *IEEE J. Solid-State Circuits*, vol. 39, no. 9, pp. 1394–1406, Sep. 2004.

[21] C. Canali, G. Majni, R. Minder, and G. Ottaviani, "Electron and hole drift velocity measurements in silicon and their empirical relation to electric field and temperature," *IEEE Trans. Electron Devices*, vol. ED-22, no. 11, pp. 1045–1047, Nov. 1975.

[22] G. Pei, J. Kedzierski, P. Oldiges, M. Ieong, and E. C.-C. Kan, "FinFET design considerations based on 3-D simulation and analytical modeling," *IEEE Trans. Electron Devices*, vol. 49, no. 8, pp. 1411–1419, Aug. 2002.

[23] *Scilab 4.x*. [Online]. Available: http://www.scilab.org

[24] R. van Langevelde, A. J. Scholten, and D. B. M. Klaassen, *Physical Background of MOS Model 11, Level 1101*, Amsterdam, The Netherlands: Koninklijke Philips Electron. N.V., Nat. Lab. Unclassified Rep. 2003/00239. [Online]. Available: http://www.semiconductors.philips.com/Philips_Models/

[25] P. K. Ko, R. S. Muller, and C. Hu, "A unified model for hot-electron currents in MOSFETs," in *IEDM Tech. Dig.*, 1981, pp. 600–603.

[26] *Synopsys Sentaurus Device Manual, Version Y-2006.06*, Synopsis Inc., Jun. 2006. [Online]. Available: http://www.synopsys.com

[27] G. D. J. Smit, A. J. Scholten, D. B. M. Klaassen, R. van Langevelde, X. Li, W. Wu, and G. Gildenblat, *PSP 102.2*, Oct. 2007. [Online]. Available: http://pspmodel.asu.edu/downloads/psp1022_summary.pdf

[28] Z. Zhu, X. Zhou, K. Chandrasekaran, S. C. Rustagi, and G. H. See, "Explicit compact surface-potential and drain-current models for generic asymmetric double-gate metal–oxide–semiconductor field-effect transistors," *Jpn. J. Appl. Phys.*, vol. 46, no. 4B, pp. 2067–2072, 2007.

[29] B. Yu, H. Lu, M. Liu, and Y. Taur, "Explicit continuous models for double-gate and surrounding-gate MOSFETs," *IEEE Trans. Electron Devices*, vol. 54, no. 10, pp. 2715–2722, Oct. 2007.

[30] G. Mugnaini and G. Iannaccone, "Physics-based compact model of nanoscale MOSFETs—Part I: Transition from drift–diffusion to ballistic transport," *IEEE Trans. Electron Devices*, vol. 52, no. 8, pp. 1795–1801, Aug. 2005.

[31] R. Thakker, N. Gandhi, M. Patil, and K. Anil, "Parameter extraction for PSP MOSFET model using particle swarm optimization," in *Proc. IWPSD*, 2007, pp. 130–133.

Venkatnarayan Hariharan (S'03) received the B.Tech. degree in electrical engineering from the Indian Institute of Technology (IIT) Bombay, Mumbai, India, in 1991 and the M.S. degree in electrical engineering from Santa Clara University, Santa Clara, CA, in 2003. He is currently working toward the Ph.D. degree in electrical engineering in the Department of Electrical Engineering, IIT Bombay.

His research interests include compact model development for FinFETs and device model development for TCAD tools.

Juzer Vasi (M'74–SM'96–F'04) received the B.Tech. degree in electrical engineering from the Indian Institute of Technology (IIT) Bombay, Mumbai, India, in 1969 and the Ph.D. degree from The Johns Hopkins University, Baltimore, MD, in 1973.

He was with The Johns Hopkins University and IIT Delhi, before moving to IIT Bombay, in 1981, where he is currently a Professor with the Department of Electrical Engineering. His research interests include CMOS devices, technology, and design. He has worked on MOS insulators, radiation effects in MOS devices, degradation and reliability of MOS devices, and modeling and simulation of MOS devices.

V. Ramgopal Rao (M'98–SM'02) received the M.Tech. degree from Indian Institute of Technology (IIT) Bombay, Mumbai, India, in 1991 and the Dr. Ingenieur degree from the Universitaet der Bundeswehr Munich, Germany, in 1997.

During 1997-1998 and again in 2001, he was a Visiting Scholar with the Department of Electrical Engineering, University of California, Los Angeles. He is currently a Professor with the Department of Electrical Engineering, IIT Bombay. He is the Chief Investigator for the Centre for Nanoelectronics Project, IIT Bombay, aside from being the Principal Investigator for many ongoing sponsored projects funded by various multinational industries and government agencies. He is also a working group member setup by the Ministry of Communications and Information Technology, Government of India on Nanotechnology. He has more than 200 publications in these areas in refereed international journals and conference proceedings. He is also the holder of two patents. His research interests include the physics, technology, and characterization of silicon CMOS devices for logic and mixed-signal applications, bio-MEMS, and nanoelectronics.

Prof. Rao is a Fellow of the Indian National Academy of Engineering and the Institution of Electronics and Telecommunication Engineers (IETE). He is an Editor for the IEEE TRANSACTIONS ON ELECTRON DEVICES in the CMOS devices and technology area and is a Distinguished Lecturer of the IEEE Electron Devices Society. He was the Organizing Committee Chair for the 17th International Conference on VLSI Design and the 14th International Workshop on the Physics of Semiconductor Devices. He serves on the program/organizing committees of various international conferences, including the 2008 International Electron Devices Meeting (IEDM), IEEE Asian Solid-State Circuits Conference, 2006 IEEE Conference on Nano-Networks, ACM/IEEE International Symposium on Low Power Electronics and Design, and 11th IEEE VLSI Design & Test Symposium, among others. He was the Chairman of the IEEE AP/ED Bombay Chapter during 2002-2003 and currently serves on the executive committee of the IEEE Bombay Section, aside from being the Vice-Chair of the IEEE Asia-Pacific Regions/Chapters Subcommittee. He was the recipient of the Shanti Swarup Bhatnagar Prize in Engineering Sciences in 2005 for his work on electron devices; the Swarnajayanti Fellowship Award for 2003-2004, instituted by the Department of Science and Technology, Government of India; the 2007 IBM Faculty Award; and the 2008 "The Materials Research Society of India (MRSI) Superconductivity & Materials Science Prize."